Journal of Applied Fluid Mechanics, Vol. 12, No. 3, pp. 701-713, 2019.
Available online at www.jafmonline.net, ISSN 1735-3645, EISSN 1735-3645.
DOI: 10.29252/jafm.12.03.28662

Study of Flow Instability in a Miniature Centrifugal Pump Based on Energy Gradient Method

K. Li[1], X. Chen[1], H. S. Dou[1†], Z. Zhu[1], L. Zheng[1] and X. Luo[2]

[1] *Faculty of Mechanical Engineering and Automation, Zhejiang Sci-Tech University 1, Hangzhou, Zhejiang 310018, China*
[2] *Thermal Engineering Department, Tsinghua University 2, Beijing, 100084, China*

†*Corresponding Author Email: huashudou@yahoo.com*

(Received December 5, 2017; accepted November 17, 2018)

ABSTRACT

Flow instability in a miniature centrifugal pump is numerically simulated with the RANS equations and the SST k-ω turbulence model. The energy gradient method is adopted to analyze the flow instability at design load and two off-design loads, and the results are compared with those analyzed by Q-criterion. The regions with large magnitude of energy gradient function (K) indicate pronounced turbulent intensity and poor flow stability. Internal flow stability is investigated in details for both the near blade surfaces region and the impeller passages. To study the mechanism of energy gradient method, internal flow parameters such as the velocity and total pressure, the transverse gradient of total mechanical energy and the work done by shear stresses are investigated respectively. The results show that the energy dissipation reaches its maximum around the leading edge of suction surface. The value of the energy gradient function K presents a different magnitude for the near blade surfaces region and the impeller passages, and the K in the impeller passage is much larger. Regions with maximum of the work done by shear stresses are concentrated on the suction surface, regions with large transverse gradient of total mechanical energy is concentrated on the hub surfaces or shroud surfaces. It is further found that the K can reflect the influence of the outer boundaries of vortex on the flow near blade surface.

Keywords: Miniature centrifugal pump; Energy gradient method; Flow instability; Total mechanical energy.

NOMENCLATURE

D	strain tensor	S	strain rate tensor
D_0	impeller inlet diameter	s	streamwise direction
D_1	impeller diameter	V	velocity
E	total mechanical energy	W	work done by shear stress
H	pump head	Z	blade number
M	torque		
N	rotating speed	τ	shear stress
n	normal direction	φ	energy dissipation rate
P	pressure	ψ	head coefficient
P_c	power coefficient	Ω	vortex tensor
Q_n	designed flow rate		
r	impeller radius		

1. INTRODUCTION

The miniature centrifugal pump is featured by the characteristic dimension of 1~50 mm, and has attracted wide attention due to its special varying sizes. It has promising application prospects, especially for liquid/gas micro-dispensing system, microfluidic system and cooling system of devices.

The miniature centrifugal pump is a key equipment of the micro-pump system, the internal flow characters inside the pump determines the

external performance of the system. Under the influence of rotating blades and the limited volute (outflow volume), flow in the centrifugal pump, especially the impeller, is complicated. The complicated flow character will further affect the flow stability and the pump operation condition. In order design a high efficiency miniature centrifugal pump, investigation on its internal flow character in depth is needed.

Investigations of internal flow of micro-pumps are commonly carried out with the particle image velocimetry (PIV) approach. The internal flow stability in centrifugal mini pump at low flow rate was studied by Wu *et al.* (2011) with the PIV measurement. They proposed that the laser induced fluorescence particle as well as the matched refractive index are the key methods to reach good PIV measurement results. Several other studies on measurement results in pumps have been introduced in Wu *et al.* (2013). Shu *et al.* (2016) investigated the Taylor vortices inside the miniature mixed-flow rotor dynamic mini pump by PIV measurement, and found that Taylor vortices could improve the mixing condition and reduce the dwell time of particles especially for regions with high shear stress.

With the numerical approach development, with the help of computational fluid dynamics (CFD) approaches, researchers have found more internal flow information. Benturki *et al.* (2018) adopts the Non-dominated Sorting Genetic Algorithm II (NSGA-II) method improved the efficiency and suction performance in a multistage pump. The internal flow pressure filed, energy characteristic and loss inside the pump is numerical studied by Li *et al.* (2016, 2016) with the SST k-ω turbulent model, and the understanding on pump energy fields, pressure fluctuations and loss characteristics is emphasized.

The inside flow characters in studied more detailed with the CFD approach. Flow condition in the back chamber is studied by Dong *et al.* (2018), and the core area behaves is carefully studied. Berten *et al.* (2009) researched the pressure fluctuation inside the impeller part and the diffuser part. The results revealed that the rotating stall yields the pressure fluctuations and the additional mechanical excitation. Han *et al.* (2017) researched the asymmetric pressure distributions and pressure fluctuations in pump by experiment. Parlak *et al.* (2018) numerical and experimental investigated the performance of a mini double discharged pump, and again proved the accurately of the CFD approach for miniature pump.

The viscosity of working fluid plays an important role in hydraulic losses in pump, Shojaeefard *et al.* (2015) and Li (2011) further investigated the hydraulic performance for impeller and volute in pump with the different viscosity fluid, and stressed the remarkable influence of fluid viscosity on internal flow and pump head.

Researchers commonly focus on the study of velocity distribution, pressure distribution and the safe operation of the pump system. Yet, the relationship between the mechanism of flow instability and internal flow characteristics are not been deeply studied.

Recently, several researchers have been working towards understanding turbulent transition and flow instability with energy gradient method. With this method, Wang *et al.* (2012) studied the instability criterion of fully developed laminar flow for the rectangular channel, and the critical Reynolds number for both the square duct and the plane Poiseuille flow were found. Investigation of the laminar to turbulent transition in ocean environment was performed by Yan (2011). He proposed that the dimensionless parameter in energy gradient method especially the energy profiles could provide a satisfactory prediction for the transition. Nowruzi *et al.* (2018) investigated the flow instability of a backward facing step flow with the energy gradient method, and valuated the local velocity, vorticity as well as the energy gradient function. Zheng *et al.* (2016, 2018) investigated the blade-tongue interaction and found that this interaction intensified the local pressure fluctuation which further intensified the local flow stability. Chen *et al.* (2018) found that the energy gradient field in the impeller could capture the features of small-scale vortices.

The present study is organized by the following sections. In section 2, the main parameters of the miniature pump, the mesh generation and its validation are presented. The energy gradient method is reviewed, and the main components in the energy gradient function is also explained in section 3. The energy gradient method is adopted to analysis the flow for both impeller passage and blade surfaces, the main components in energy gradient function are further investigated separately in section 4. Results of energy gradient method are compared with those analyzed by *Q*-criterion (Jeong *et al.*, 1995) are also presented in section 4. The paper end with the conclusions in section 5.

2. MODEL OF THE CENTRIFUGAL PUMP AND MESH ENERATION

2.1 Main Pump Parameter

The miniature pump studied in this paper is designed for fluid transportation in micro devices. Figure 1 gives the model of miniature centrifugal pump. The miniature centrifugal pump has 5 backward blades and the design volume flow rate at the nominal rotational speed of 8000 revolutions per minute is 0.48 m^3/h. Inlet diameter of the impeller is 13 mm, while the impeller diameter is 33 mm. The outlet diameter of the eccentric-design volute is 10 mm. There is a gap between the impeller and the back chamber of approximately 0.5 mm, which provide a source of the impeller suspending while further caused the local high shear stress. Short summary of the miniature centrifugal pump is presented in Table 1.

Numerical simulations of the miniature centrifugal

pump are performed in ANASY-CFX, and the SST k-ω turbulent model is adopted to describe the turbulence characteristics of internal flow. The analysis type is set as the steady state. And in the physics definition, the fluid is set as the water. At the inlet, different inflow volume flow rate is given to change the operation point. The turbulence intensity at the inlet boundary is 5%. The total pressure is given as 101325 Pa and normal to the outlet boundary.

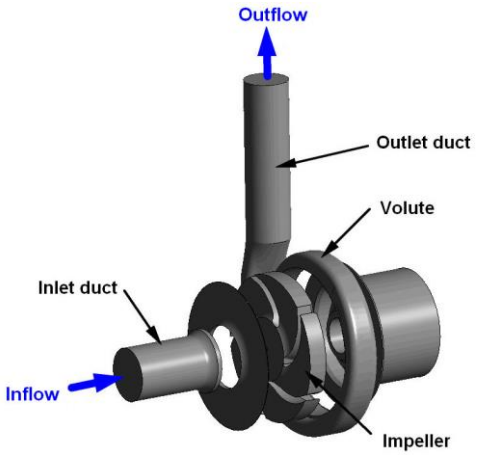

Fig. 1. Model of the centrifugal pump.

Table 1 General Parameters of the Pump

Parameter	Value
Designed flow rate Q_n(m^3/h)	0.48
Head H(m)	11.5
Rotating speed N(rpm)	8000
Blade number Z	5
Impeller inlet diameter D_0(mm)	13
Impeller diameter D_1(mm)	33

The fluid domain is divided into five components, composed of four stationary domains and one rotating domain. Frozen-rotator interfaces have been generated for the rotating impeller and the stationary components (inlet and volute). The pitch angle for the components are 360 degree. The physical timescale is set as the automatic approach, and the Non-slip condition is applied to the walls.

2.2 Mesh Generation and Its Validation

The grid elements for all component were produced with ANSYS ICEM. And the structured mesh is adopted in the inlet, front chamber, impeller and the back chamber, the refined unstructured mesh is generated in the volute. Mesh for small gaps in the miniature centrifugal pump, is refined, such as the clearance in the front chamber includes 8 layers and the clearance between the impeller and the back chamber includes 8 layers. The mesh details can be seen in Fig. 2.

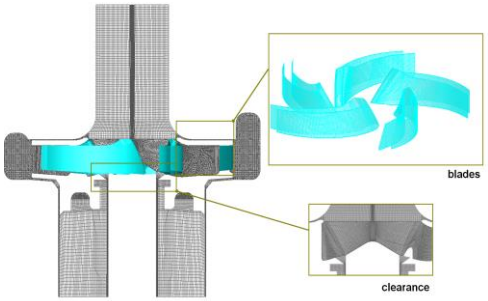

Fig. 2. Grid view of the miniature pump.

The grid validation is carried out under the design load at volume flow rate Q_n=0.48 m^3/h and the rotating speed N=8000 rpm. The tested grid numbers are 2.87 million, 4.31 million, 6.68 million and 10.8 million, respectively. Then, the non-dimensional head coefficient ψ and the power coefficient P_c are selected to verify the four sets of mesh.

The non-dimensional head coefficient ψ is defined as

$$\psi = \frac{gH}{N^2 r^2} \tag{1}$$

where r is the outer radius of the impeller.

The power coefficient P_c can be expressed as

$$P_c = \frac{M \times N}{\rho N^3 r^5} \tag{2}$$

where ρ is the fluid density and M denotes the measured torque.

Table 2 Mesh Validation

Cases (million)	ψ	Relative change	P_c	Relative change
2.87	1.701E-3	-1.46%	1.952E-5	-3.12%
4.31	1.676E-3	-0.59%	1.891E-5	-2.59%
6.68	1.666E-3	-0.30%	1.842E-5	-0.16%
10.8	1.661E-3	/	1.839E-5	/

As shown in Table 2, variations of the calculated flow parameters for four grids are given. With the grid number increasing, relative change of head coefficient is -1.46% for 4.31 million, -0.59% for 6.68 million and -0.30% for 10.8 million. Relative change of power coefficient is -3.12% for 4.31 million, -2.59% for 6.68 million and -0.16% for 10.8 million. Relative change of ψ and P_c do not vary much with increasing grid number. To balance the computational cost and accuracy of the results, the case with 6.68 million cells is chosen for the following simulations. The Y plus condition is present in Fig. 3 with the grid number 6.68 million, the Y+ of the overall model is 0~45, and is 0~20 of the impeller domain. The Y plus is well agreed with the requirement of the SST k-ω turbulent model.

3. ENERGY GRADIENT METHOD REVISIT

In recent years, Dou and co-authors (Dou, 2006; Dou and Nhan, 2007; Dou *et al.*, 2008; Dou and Khoo, 2010) proposed the energy gradient method to investigate the turbulent transition and the flow instability. According to this method, the internal flow field is regarded as an energy field, regions with maximum of this function are the most dangerous positions to initiate the instability.

For a given pressure driven flow, the function can be expressed as:

$$K = \frac{\partial E / \partial n}{\partial E / \partial s} \tag{3}$$

For a given shear driven flow, the function can be expressed as:

$$K = \frac{\partial E / \partial n}{\partial h / \partial s} \tag{4}$$

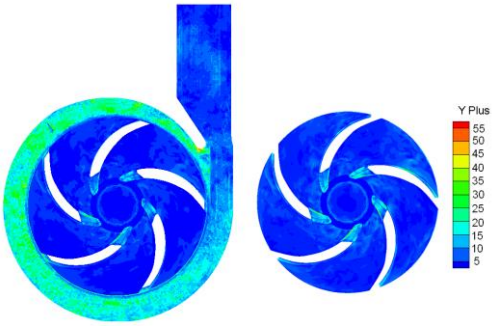

Fig. 3. Y plus condition for miniature pump.

Here, s presents the streamwise direction along the streamline, and n denotes the normal direction of the streamline. Every streamline can be project into three Cartesian planes which are perpendicular to each other. And the function K is approximated as the summation for the three Cartesian planes characters. Namely, the s and n are specified for the streamline on every Cartesian plane. Character E is the total mechanical energy for per unit volumetric fluid particle, and h is the friction loss along the streamline for a finite length.

For the flow where the pressure driven flow as well as the shear driven flow are simultaneously exists, Dou (2017) proposed a universal equation, and the function can be expressed as:

$$K = \frac{V\left(\partial E / \partial n\right)}{V\left(\partial W / \partial s\right)} = \frac{\sqrt{u_i^2}\sqrt{\left(\dfrac{\partial E}{\partial n}\right)_i^2}}{\sqrt{u_i^2}\sqrt{\left(\dfrac{\partial E}{\partial s}\right)_i^2} + \varphi} \tag{5}$$

The φ is the energy dissipation induced by viscosity, and can be expressed as:

$$\varphi = 2\mu\left[\frac{1}{2}\left(\nabla V + \nabla V^T\right)\right]^2 = 2\mu\left[\frac{1}{2}\left(\frac{\partial u_j}{\partial x_i} + \frac{\partial u_i}{\partial x_j}\right)\right]^2 \tag{6}$$

For function K, $V\left(\partial E / \partial n\right)$ denotes the transverse gradient of mechanical energy and the $V\left(\partial W / \partial s\right)$ denotes the work done by shear stresses. The function K is a dimensionless field function that expresses the flow instability intensity. As is present, the function K can be regarded as a ratio of the energy and the energy loss.

Parameters of function K are studied in details. Total mechanical energy gradient and the work done by shear stress are investigate to study the regions with high total mechanical energy and high energy loss in pump. Finding the regions with high energy gradient and high energy loss is beneficial to provide theoretical guidance and give an optimized guide when a new pump is designed. In this paper, the energy gradient function K and the related quantities are calculated by in-house code

4. RESULTS AND DESCRIPTION OF REFERENCES

The head and efficiency performance curves of the miniature pump is presented in Fig. 4. According to Fig. 4, we can found that with flow rate increase, the pump head is increasing in low flow rate regime, while head is decreasing in high flow rate regime. The head-flow rate (H-Q) curve shows a hump-like distribution, which is prone to induce flow instability for flow rate at off-design conditions. To deep investigate the internal reason of the hump-like character, in the presented work, study of flow stability is carried out under three different flow rates. That is the low flow rate at Q/Q_n=0.6, design condition Q/Q_n=1.0 and high flow rate at Q/Q_n=1.4.

Fluid particles in impeller are forced to rotate together by the impeller blades, which further intensified the complexity. Also, the flow parameters of blade surfaces and impeller passage is different and interacted. In order to provide a comprehensive study about the internal flow stability inside the impeller, the characteristics of flow in the impeller passage as well as the flow characteristics for blade surfaces are studied in the following sections.

In order to illustrate the flow parameter for each blade and impeller passage, as presented in Fig. 5, five impeller passages are labeled from passage A to passage E, and five blades are labeled as blade 1 to blade 5, respectively. Curves on blade surfaces are the intersection lines of blade surfaces and middle span plane. In this paper, data of flow parameters of blade surface are obtained from the ten curves shown in Fig. 5(b).

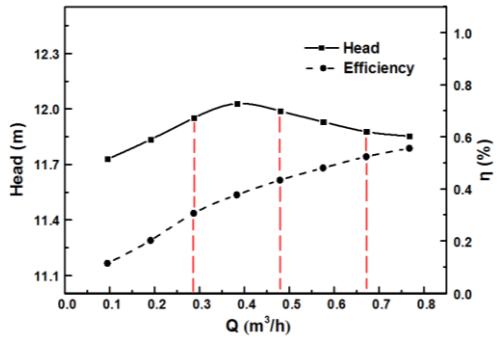

Fig. 4. Head curve of the centrifugal pump.

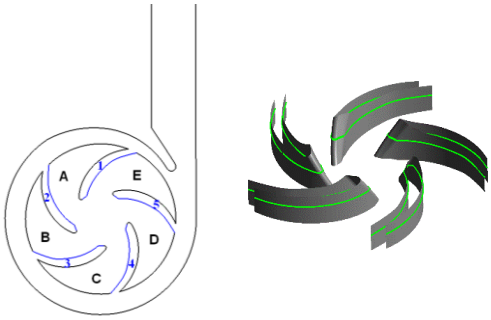

(a) Impeller passage (b) Curves on blade surface

Fig. 5. The impeller passage and curves on blades.

4.1 Analysis of Basic Flow Condition and Energy Dissipation

In Figs. 6(a), (b) and (c), velocity reaches its minimum in middle region of suction surface and blade outlet near the tongue, which leads the local condition to be more complex. Shedding vortices in the middle position of passage E are emerged near the blade trailing edge, while shedding vortices in passage D are much closer to the blade suction surface. The large scale vortex in passage D is mainly affected by the tongue. With the flow rate increasing from $0.6Q_n$ to $1.4Q_n$, separation vortices shown in passage D tend to weaken and migrate to the impeller exit. Moreover, there is a dramatic changes of cross-sectional area for the asymmetric volute, it caused the emerge of the strong vortices in passage E which present different vortex intensities under different flow rates. Meanwhile, the strong "jet-wake" structure, affected by the high impeller rotating speed, exists at the impeller outlet.

In Figs .6(d), (e) and (f), low pressure fields appear near the blade leading edge of the suction surface. Affected by the jet-wake structure, local total pressure in the jet-wake fields reach a relatively low value. As may be seen, the inverse pressure gradient fields in passage D and passage E have exacerbated the local flow separation. Especially for $0.6Q_n$ and $1.4Q_n$, the sharp inverse pressure gradient in middle passage E has enhanced the separation of vortices. Regions with sharp inverse pressure gradient indicate a poor local pressure field, and those regions are consistent with the outer boundaries of separating vortices.

Figure 7 shows the energy dissipation caused by viscosity, which represents the internal flow frictional loss intensity. Due to the direct contact between blade surfaces and fluid particles, analysis about energy dissipation on both suction surface and pressure surface is needed. Affected by the curvature of impeller blade, especially its strong geometric influence, energy dissipation (φ) reaches it maximum φ_{max} (the subscript "max" denotes the large region) at blade leading edge. It indicates the high energy dissipation and complex flow condition around leading edge. Regions with φ_{max} near blade leading edge are enlarging form $0.6Q_n$ to $1.4Q_n$. Meanwhile, regions with φ_{max} on suction surface is weakened along the streamwise direction, and φ_{max} on pressure surface tends to move to the blade trailing edge.

As can be seen, the energy dissipation on pressure surface is stronger than that on suction surface under same flow rate. The vortices, especially its outer boundaries, will worsen the local velocity field and intensified local friction loss. In Fig. 7, regions with φ_{max} on pressure surface of blade 5 have reflected this influence of vortices outer boundaries.

Figure 8 depicts the distribution of φ on both suction surface (first column) and pressure surface (second column). For fields near the blade leading edge, the change of attack angle and the shedding vortices intensified the local energy dissipation, which can be seen form the φ_{max} at [0, 0.1]. The forced separation of vortices are then detached form the leading edge surface, and resulting in the decreasing of φ at [0.1, 1]. Different with the suction surface, regions with φ_{max} on pressure surface is affected by the strong fluid particle friction and the strong large scale vortex outer boundaries. The two φ_{max} emerged in pressure surface can be well illustrate the influence on the strong large scale vortex outer boundaries.

4.2 Energy Gradient and Work Done by Shear Stress

In this section, study of regions with maximum of transverse gradient of mechanical energy $V\left(\partial E/\partial n\right)$ and with maximum of work done by shear stresses $V\left(\partial W/\partial s\right)$ are presented separately. To preserve the main instability fields in impeller, the thresholds of $V\left(\partial E/\partial n\right)$ and $V\left(\partial W/\partial s\right)$ adopt the value of 2×10^8 as the criterion in this paper.

In Figs. 9(a), (b) and (c), fields with maximum of $V\left(\partial E/\partial n\right)$ are mainly concentrate in middle area on suction surface and hub/shroud surfaces of impeller passage. It indicates that strong energy change exists in the leading edge of the suction surface, the "jet-

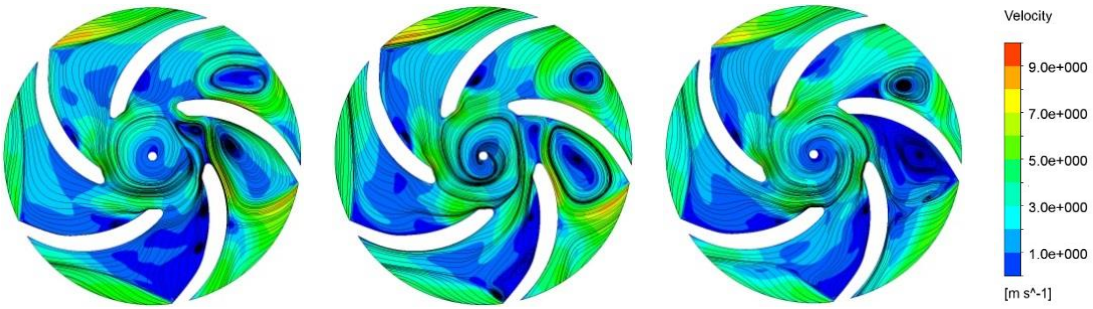

(a) 0.6Q_n (b) 1.0Q_n (c) 1.4Q_n

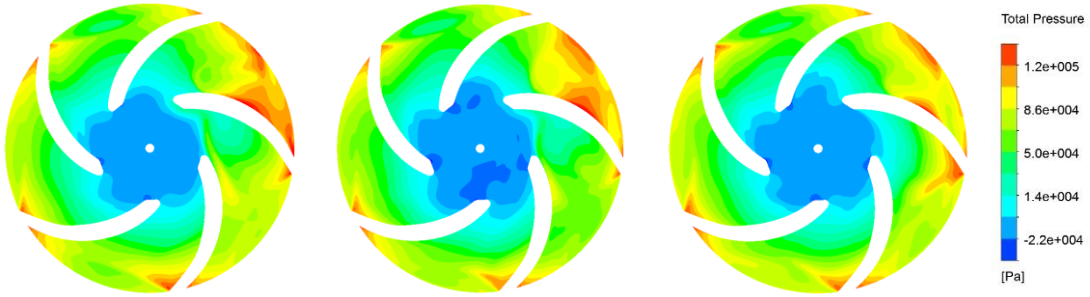

(d) 0.6Q_n (e) 1.0Q_n (f) 1.4Q_n

Fig. 6. Distribution of relative velocity (first column) and total pressure (second column) on center plane.

(a) 0.6Q_n (b) 1.0Q_n (c) 1.4Q_n

Fig. 7. Distribution of φ on the blade surfaces at (a) 0.6Q_n, (b) 1.0Q_n and (c) 1.4Q_n.

wake" structure and outer boundaries of vortex. Different with $V\left(\partial E/\partial n\right)$, fields with maximum of $V\left(\partial W/\partial s\right)$ are mainly concentrated on blade surfaces, and reaches its maximum at leading edge on suction surface. It indicates that internal flow field near the blade leading edge on suction surface is unstable with high energy loss. In Figs. 9(d), (e) and (f), regions with maximum of $V\left(\partial W/\partial s\right)$ emerge at the exits of passage D and passage E , which is consistent with the distribution of the large scale vortices. It illustrates that the outer boundaries of vortex will enhance the shear stress density and will intensify the energy loss caused by shear stresses.

The span distribution of regions with maximum of $V\left(\partial E/\partial n\right)$ and $V\left(\partial W/\partial s\right)$ are presented in Fig. 10. It is notable that in Figs. 10(a) and (d), ring areas with large value of $V\left(\partial E/\partial n\right)$ and $V\left(\partial W/\partial s\right)$ are presented at 0.1 span plane. This ring area is near the physically clearance of impeller and back chamber. It indicates that the flow field near this clearance has a high energy gradient, strong shear stress and high energy loss. Further, fields with maximum of $V\left(\partial E/\partial n\right)$ and $V\left(\partial W/\partial s\right)$ for 0.1 span (near impeller hub) and 0.9 span (near impeller shroud) is much strong than that for 0.1 span (the center plane), which indicates a different total mechanical energy and the shear stress condition.

The blade leading edge have enhanced the forced

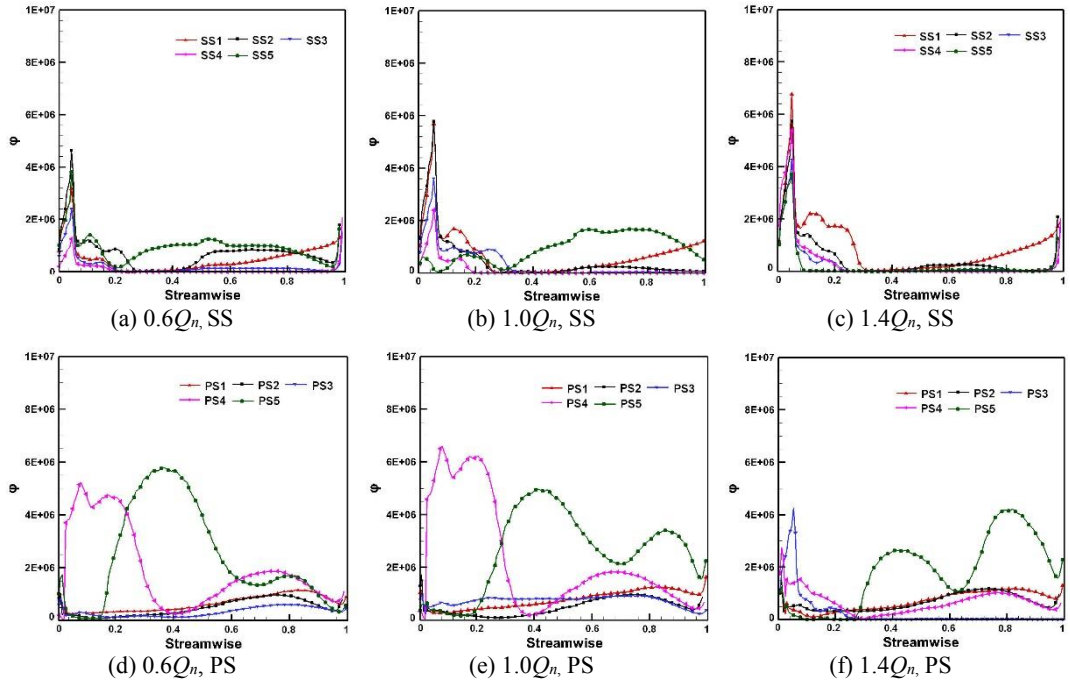

(a) $0.6Q_n$, SS (b) $1.0Q_n$, SS (c) $1.4Q_n$, SS

(d) $0.6Q_n$, PS (e) $1.0Q_n$, PS (f) $1.4Q_n$, PS

Fig. 8. Distribution of φ on suction surface (first column) and pressure surface (second column).

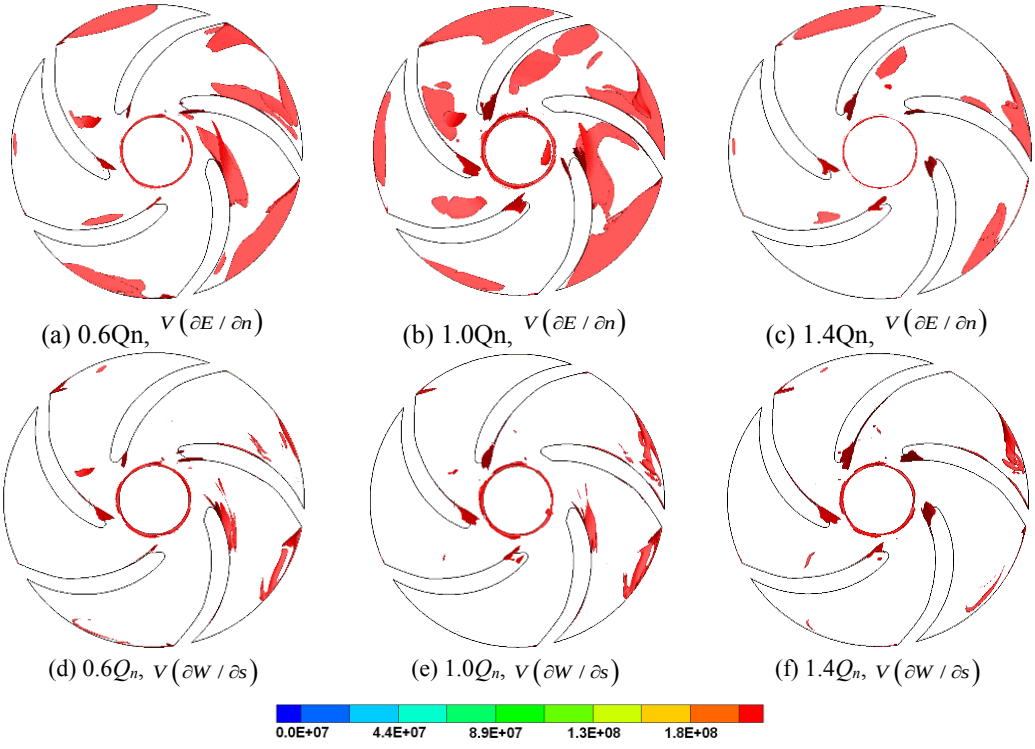

(a) 0.6Qn, $V\left(\partial E/\partial n\right)$ (b) 1.0Qn, $V\left(\partial E/\partial n\right)$ (c) 1.4Qn, $V\left(\partial E/\partial n\right)$

(d) $0.6Q_n$, $V\left(\partial W/\partial s\right)$ (e) $1.0Q_n$, $V\left(\partial W/\partial s\right)$ (f) $1.4Q_n$, $V\left(\partial W/\partial s\right)$

Fig. 9. ISO-surface of $V\left(\partial E/\partial n\right)$ (first column) and $V\left(\partial W/\partial s\right)$ (second column).

separation of vortices, these vortices flow into the impeller passages and further intensified the local flow stability. Also, the vortices generation and separation have enhanced this uneven distribution of total mechanical energy transverse gradient. Investigation of the total mechanical energy transverse gradient on the blade surfaces is presented in Fig. 11. As shown in Figs. 11(a), (b) and (c), the $V\left(\partial E/\partial n\right)$ on suction surface tends to increase with the flow rate increase. Under same flow rate, the maximum of $V\left(\partial E/\partial n\right)$ on the suction surface is larger than that on pressure surface. The maximum

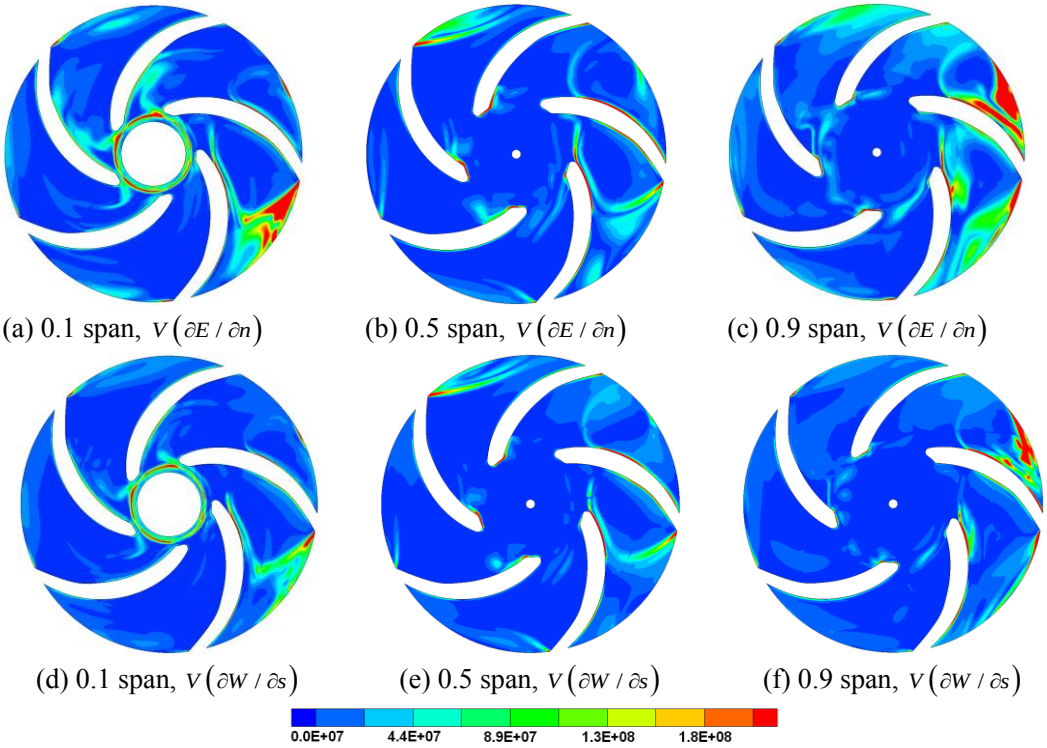

Fig. 10. Span distribution of $V(\partial E/\partial n)$ (first column) and $V(\partial W/\partial s)$ (second column) at 1.0Q_n.

of $V(\partial E/\partial n)$ on suction surface is mainly located at the position of [0, 0.2], while it is [0.1, 0.3] on pressure surface.

Affected by the shedding vortices in impeller passage, the maximum of $V(\partial E/\partial n)$ is mainly concentrated on the middle area on pressure surface. In Fig. 11 (d), (e) and (f), fields with the maximum of $V(\partial E/\partial n)$ on pressure surface are lag behind its on suction surface. In Figs. 11(d) and (e), it can be found that the value of $V(\partial E/\partial n)$ for blade 4 and 5 is larger than that for blade 1-3. It can be illustrated as the vortices existing in passage D and passage E have enhanced the local energy gradient distribution. In Fig. 11(f), the high energy gradient of blade 3 is mainly affected by the negative attack angle at 1.4Q_n.

Figure 12 gives the investigation about the work done by shear stresses on blade surfaces. Combine Fig. 8 (the energy dissipation), it can be seen that the energy dissipation is one of the main reasons of energy loss. The energy dissipation and energy loss caused by shear stress, for all conditions, exhibited a very similar patterns and trends.

Note that, in Figs. 12(a), (b) and (c), distribution of $V(\partial W/\partial s)$ is similar to that for φ. Its maximum on suction surface is mainly located at [0, 0.1], which is caused by the forced separation of vortices. Meanwhile, the value of $V(\partial W/\partial s)$ on suction surface is larger than that on pressure surface, especially for flow field near the blade leading edge. As presented in Figs. 12(d), (e) and (f), two regions with local maximum of $V(\partial W/\partial s)$ on pressure surface, certified the strong dissipation and energy loss caused by the separation of vortices, are in good agreement with the outer vortex boundary. Vortices in passage D and E have changed the local shear stress distribution, and then influences the work done by shear stress. It's worth noting noted that regions with the maximum of $V(\partial W/\partial s)$ on pressure surface tends to move backward with the flow rate increase, which simultaneously indicates the large scale vortex is moving near to the impeller outlet.

4.3 Energy Gradient Function and *Q*-Criterion

In this section, the energy gradient function *K* and the *Q* from *Q*-criterion are adopt to study the internal flow character for both blade surfaces and impeller passages. According to the energy gradient method, the *K* is represented as a ratio and is used to locate the flow instability fields. In energy gradient method, the total mechanical energy gradient is regarded as a critical parameter. Considering the total mechanical energy consist the velocity and the pressure, which indicates that in its definition, the *K* is affected by both the intensity of energy gradient and the intensity of shear stresses.

According to the energy gradient theory, regions with the larger value of function *K* is more likely lose the flow stability. To preserve the main instability fields in impeller passage, the thresholds of function *K* adopts the value of 30 as the criterion in this paper, the function *K* takes as the K_{max} when $K \geq 30$.

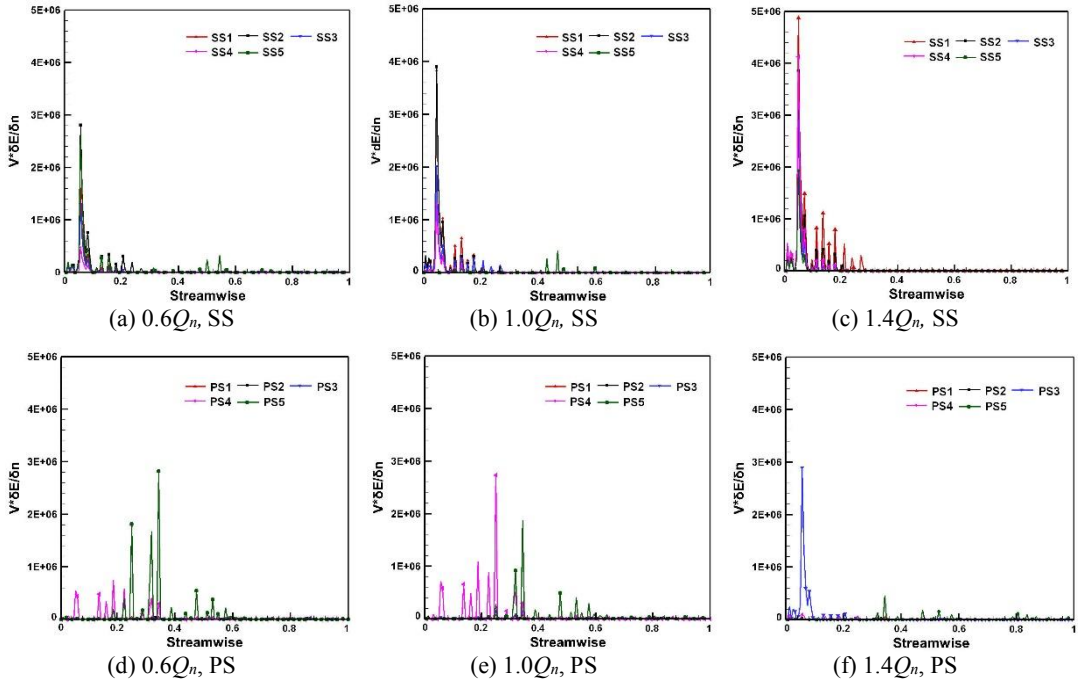

(a) 0.6Q_n, SS (b) 1.0Q_n, SS (c) 1.4Q_n, SS

(d) 0.6Q_n, PS (e) 1.0Q_n, PS (f) 1.4Q_n, PS

Fig. 11. Distribution of $V\left(\partial E/\partial n\right)$ on suction surface (first column) and pressure surface (second column).

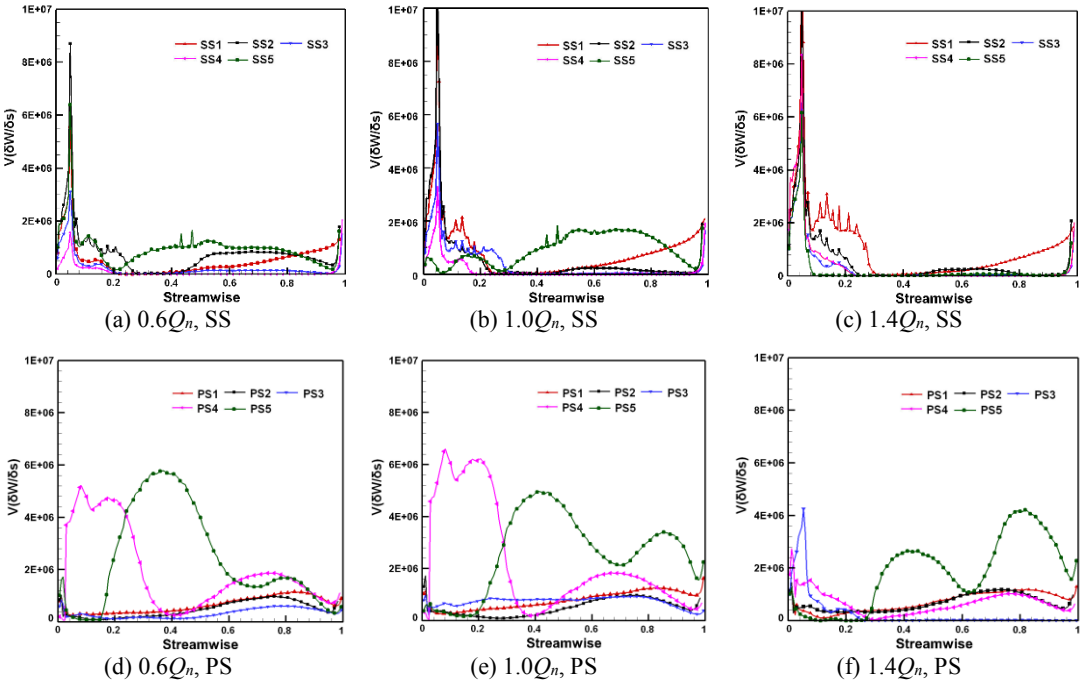

(a) 0.6Q_n, SS (b) 1.0Q_n, SS (c) 1.4Q_n, SS

(d) 0.6Q_n, PS (e) 1.0Q_n, PS (f) 1.4Q_n, PS

Fig. 12. Distribution of $V\left(\partial W/\partial s\right)$ on suction surface (first column) and pressure surface (second column).

Fields with K_{max} is the fields where the transverse gradient of mechanical energy more than 30 times of the work done by shear stress.

The iso-surface of K is presented in Figs. 13(a), (b) and (c). Combined with the relative velocity distribution shown in Fig. 6, fields of the K_{max}, seen in Fig. 13, are mainly located at the exit of impeller passage, showing a vortex distribution in passage D and passage E. Regions with K_{max} has a good agreement with the "jet-wake" structure and the outer boundaries of vortices shown in passage D and passage E. It indicates that the K could locate flow instability fields caused by the strong shear stress in

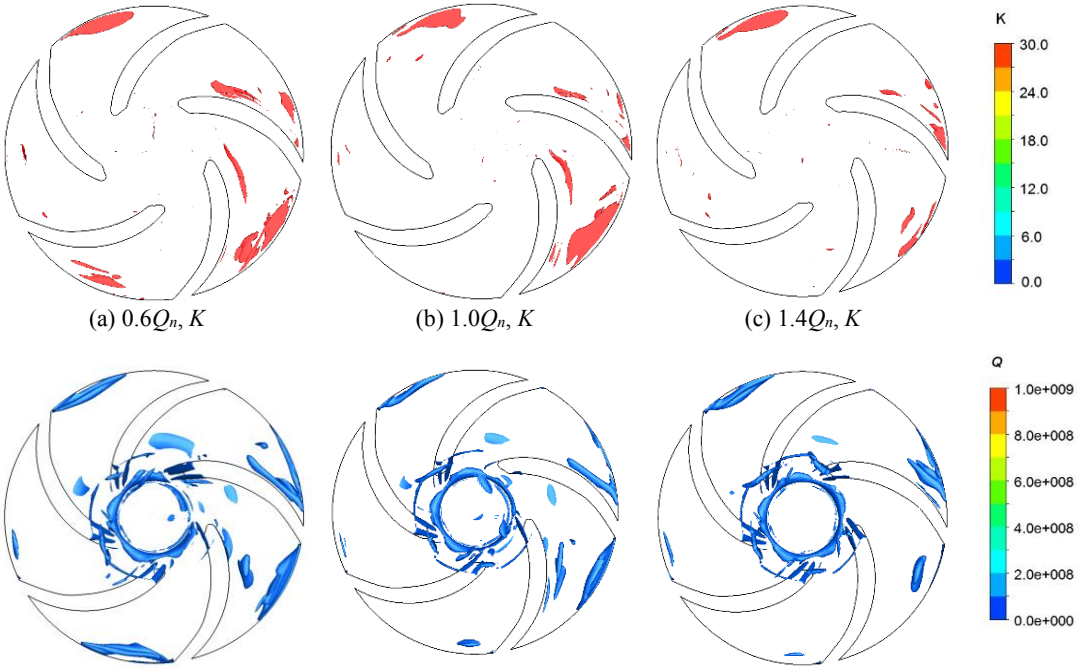

(a) 0.6Q_n, K (b) 1.0Q_n, K (c) 1.4Q_n, K

(d) 0.6Q_n, Q (e) 1.0Q_n, Q (f) 1.4Q_n, Q

Fig. 13. ISO-surface of *K* (first column) and *Q* (second column) in impeller.

vortex outer boundaries. Moreover, strong shear layers inside the "jet-wake" structure and its corresponding flow instability are also located by function *K*. Regions with the K_{max} tend to shrinking with the flow rate increase, which indicates the corresponding flow instability is debilitating.

The *Q*-criterion is employed to study the instability of flows. It is defined as:

$$Q=\frac{1}{2}\left(\left\|\Omega^2\right\|-\left\|S^2\right\|\right) \tag{7}$$

where S represents strain rate tensor, and Ω is the vortex tensor, and the two parameter can be expressed as:

$$\Omega_{ij}=\frac{1}{2}\left(\frac{\partial u_i}{\partial x_j}-\frac{\partial u_j}{\partial x_i}\right) \tag{8}$$

$$S_{ij}=\frac{1}{2}\left(\frac{\partial u_i}{\partial x_j}+\frac{\partial u_j}{\partial x_i}\right) \tag{9}$$

Parameter S and Ω in the *Q*-criterion represent the symmetric and antisymmetric parts of the velocity gradient tensor, which denote the deformation and rotation of the flow field, respectively. For *Q*-criterion, fields where meet the two requirements can be regarded as fields dominated by rotation: (a) the value of Q satisfied $Q>0$, (b) the pressure of the position reaches the minimum value around the flied. To preserve the main vortex structure in impeller passage, the thresholds of *Q*-criterion adopts $Q = 1 \times 10^8$ as the criterion.

As shown in Figs. 13(d), (e) and (f), the "jet-wake" structure and the vortices, shown in passage D and passage E, are accompanied with the huge vortex intensity. These fields are well captured by the Q_{max}. Note that there is inner ring region with the Q_{max}, and this field near the clearance of the impeller and back chamber. It can be illustrated that filed near this clearance exists a frequent flow change between the impeller and the back chamber, which further induced the high shear stress intensify in the local region. With the high speed impeller, the high stress intensity region can be further regarded as a rotation-dominated field. This ring region is also well captured by the $V\left(\partial W/\partial s\right)$, seen in Fig. 9 and Fig. 10. Due to the function K is affected by both energy gradient and the intensity of shear stress. The instability caused by energy gradient and shear stress near the interface, shown in Fig. 9, have a similar intensity, which further causes that the K in regions near the interface is relatively low.

Note that passages D and passage E show a significant change in vortex structure, and the two passages are selected to study the capacity of K and Q conditions on blade surface. As corresponding, flow parameters of blade 1, blade 4 and blade 5 are studied.

As shown in Fig. 14 and Fig. 15, the K on blade surfaces present a different magnitude with that for impeller passages. The K_{max} on blade surface is much smaller than that for impeller passage. The outer boundaries of vortices with strong shear layer could intensify the local velocity and pressure field. Further, the changed local velocity as well as the pressure field induced a poorer flow stability on blade surfaces. In Fig. 14, regions with the K_{max} on suction surface are mainly concentrated at relative position of [0, 0.2]. At the position of [0.2, 1], the

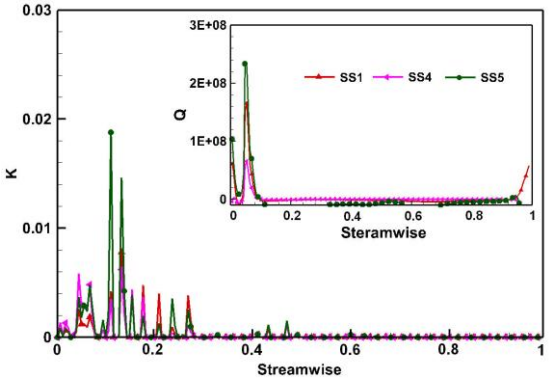

(a) $0.6Q_n$, SS

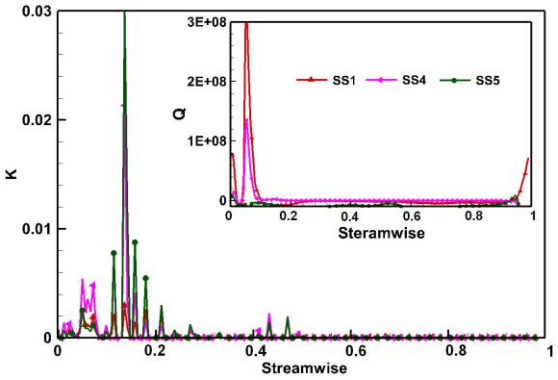

(b) $1.0Q_n$, SS

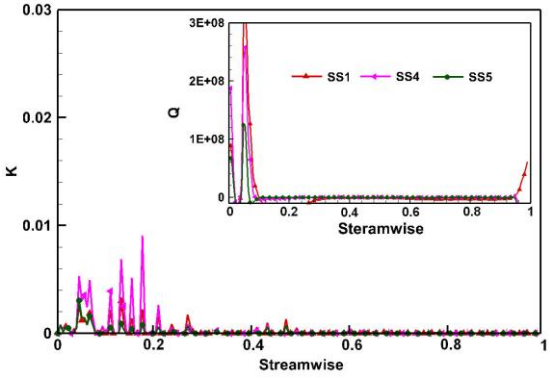

(c) $1.4Q_n$, SS

Fig. 14. Distribution of *K* and *Q* on suction surface at (a) $0.6Q_n$, (b) $1.0Q_n$ and (c) $1.4Q_n$.

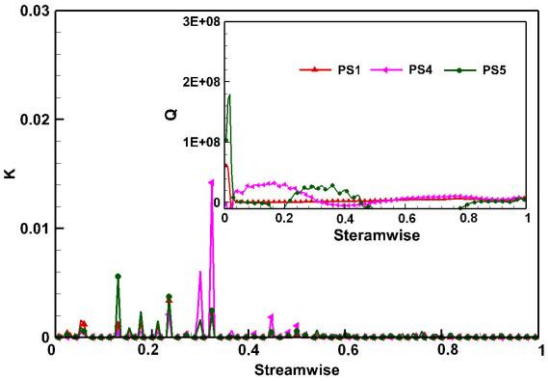

(a) $0.6Q_n$, PS

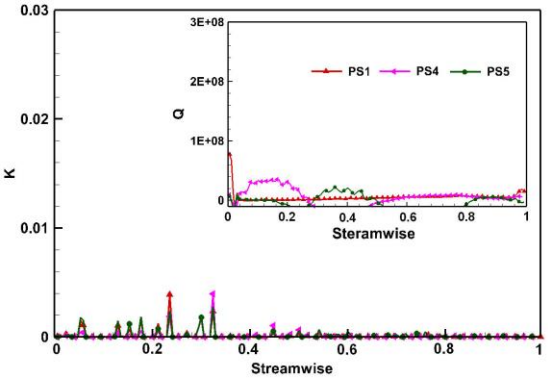

(b) $1.0Q_n$, PS

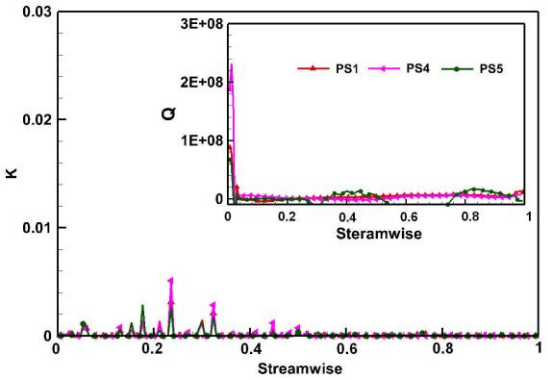

(c) $1.4\ Q_n$, PS

Fig. 15. Distribution of *K* and *Q* on pressure surface at (a) $0.6Q_n$, (b) $1.0Q_n$ and (c) $1.4Q_n$.

vortices shedding from the blade leading edge are detached form the blade, and reduced its influence on blade surface, which further corresponding enhanced the flow stability on suction surface. The enhanced flow stability for regions away from blade leading edge is reflected by the small value of K at [0.2, 1]. Moreover, the K_{max} on suction surface tends to shrink smoothly from $0.6Q_n$ to $1.4Q_n$. With flow rate increases, the change of K_{max} value reflected the flow stability on suction surface is stronger in high flow rate zone than that in small flow rate zone.

The Q_{max} at the relative position of [0, 0.1] indicates that a strong rotating dominated field are exist near the blade leading edge, which can be illustrated as the strong separation of leading edge. With the vortices shedding from surface, the intensity of vortex is also reduced, which further induced the Q at [0.1, 1] is relative smooth and small. As shown in Fig. 14, the distribution of Q is different from that for the K, particularly for blade 5 suction surface. It can be illustrated that the different for blade 5 suction surface is affected by large scale vortices outer boundaries, which have changed the local velocity field of blade 5 surface.

The distribution of the K and the Q on pressure is given in Fig. 15. Under different flow rates, the K_{max}

on pressure surface is mainly concentrated at the relative position of [0.1, 0.3]. The K is decreasing with the flow rate increase from $0.6Q_n$ to $1.4Q_n$. It indicates that the instability locates at the relative position of [0.1, 0.3] and the internal flow tends to be more stable with flow rate increase. In Fig. 15(a), the K_{max} for blade 4 is larger than that for blade 1 and blade 5. The vortex intensity near blade 4 under 0.6 Q_n is much stronger than other flow rates, which induced the K_{max} of blade 4 has a larger value than that for blade 1 and blade 5. Meanwhile, under the same flow rate, the Q on blade pressure surface is smaller than that on suction surface.

In Fig. 15, the Q_{max} is mainly located at the relative position of [0, 0.05], it means that rotation-dominated field exists near the area of [0, 0.05]. The two relatively large values of Q at [0.05, 0.4] indicates two regions with strong rotation intensity exist on the middle pressure surface. From the distribution of K and the Q on suction surface and pressure surface, the most dangerous places for the two sides of blade are not absolutely the same. The relatively minimum of both K and Q on pressure surface indicate the internal flow on pressure surface is more stable than suction surface.

5. CONCLUSIONS

The internal flow characteristics and flow stability of a miniature centrifugal pump impeller are analyzed by energy gradient method. The physical mechanism of energy gradient method is explored through the study of the performance of total mechanical energy gradient and the work done by shear stress. Main conclusions can be summarized as follows:

1. The energy gradient function K have different performance, and the K has a larger value in impeller passage than that on blade surfaces. And the fields on the pressure surfaces, accompany with the minimum K, is most stable.
2. The energy dissipation has a strong effect on energy loss, and reaches its maximum around the leading edge on suction surface. Fields with maximum of work done by shear stresses are mainly concentrated on suction surface; fields with high energy gradient are mainly concentrated on the bub surface and shroud surfaces. These factors make the flow to be more stable on pressure surface, and to be more unstable at hub or shroud surfaces and suction surface leading edge.
3. The K and Q have different distributions on blade surfaces. The K_{max} is mainly located at [0, 0.2] on suction surface and [0.1, 0.3] on pressure surface, while maximum of Q is [0, 0.1] and [0, 0.4] respectively. The K locates the instability regions caused by the outer boundaries of vortex on the blade surfaces, while the Q present the rotating domain fields.

ACKNOWLEDGMENT

This work is supported by National Natural Science Foundation of China (51536008, 51579224), Zhejiang Province Key Research and Development Plan Project (2018C03046), and the Natural Science Foundation of Zhejiang Province (LQ16E090005).

REFERENCES

Benturki, M., R. Dizene and A. Ghenaiet (2018). Multi-objective optimization of two-stage centrifugal pump using NSGA-II algorithm, *Journal of Applied Fluid Mechanics* 11(4), 929-943.

Berten, S., P. Dupont, L. Fabre, M. Kayal, F. Avellan and M. Farhat (2009). Experimental investigation of flow instabilities and rotating stall in a high-energy centrifugal pump stage. *Proceedings of ASME 2009 fluids engineering division summer meeting*, Colorado, USA.

Chen, X. P., Z. C. Zhu, H. S. Dou and Y. Li (2018). Large eddy simulation of energy gradient field in a centrifugal pump impeller. *Proc IMechE, Part C: J Mechanical Engineering Science*.

Dong, W. and W. L. Chu (2018). Numerical investigation of fluid flow mechanism in the back-shroud cavity of a centrifugal pump. *Journal of Applied Fluid Mechanics* 11(3), 709-719.

Dou, H. S. (2006). Mechanism of flow instability and transition to turbulence. *International Journal of Non-Linear Mechanics* 41(4), 512-517.

Dou, H. S. (2017). A universal equation for calculating the energy gradient function in the energy gradient theory. *Proc. of ICCHMT*, Seoul, Korea.

Dou, H. S. and B. C. Khoo (2010). Criteria of turbulent transition in parallel flows. *Modern Physics Letters B* 24(13), 1437-1440.

Dou, H. S. and P. T. Nhan (2007). Viscoelastic flow past a confined cylinder: Instability and velocity inflection. *Chemical Engineering Science* 62(15), 3909-3929.

Dou, H. S., B. C. Khoo and K. S. Yeo (2008). Instability of Taylor–Couette flow between concentric rotating cylinders. *International Journal of Thermal Sciences* 47(11), 1422-1435.

Han, L., H. J. Wang, Y. H. Gao, D. Y. Li, R. Z. Gong, and X. Z. Wei (2017). Dynamic simulation in guide vane opening process of a pump-turbine in pump mode. *Journal of Applied Fluid Mechanics* 10(5), 1441-1449.

Jeong, J., F. Hussain and F. Hussain (1995). On the identification of a vortex. *Journal of Fluid Mechanics* 285, 69-94.

Li, D. Y., R. Z. Gong, H. J. Wang, J. Zhang, X. Z. Wei and L. F. Shu (2016). Numerical investigation in the vanned distributor under different guide vanes openings of a pump turbine in pump mode. *Journal of Applied Fluid Mechanics* 9(1), 253-266.

Li, D. Y., R. Z. Gong, H. J. Wang, X. Z. Wei, Z. S. Liu and D. Q. Qin (2016). Analysis of rotor-stator interaction in turbine mode of a pump-turbine model. *Journal of Applied Fluid Mechanics* 9(5), 2559-2568.

Li, W. G. (2011). Blade exit angle effects on performance of a standard industrial centrifugal oil pump. *Journal of Applied Fluid Mechanics* 4(3), 105-119.

Nowruzi, H., S. Nourazar and H. Ghassemi (2018). On the instability of two dimensional backward-facing step flow using energy gradient method. *Journal of Applied Fluid Mechanics* 11(1), 241-256.

Parlak, Z., M. Kemerli, T. Engin and Y. Koc (2018). Design of a mini double-discharge centrifugal pump under multiphase flow by CFD and experimental verification. *Journal of Applied Fluid Mechanics* 11(5), 1443-1454.

Shojaeefard, M. H., B. S. Rizi, A. Khalkhali and M. Tahani (2015). A new method to calculate centrifugal pump performance parameters for industrial oils. *Journal of Applied Fluid Mechanics* 8(4), 673-681.

Shu, F., R. Tian, S. Vandenberghe and J. F. Antaki (2016). Experimental study of micro-scale taylor vortices within a co-axial mixed-flow blood pump. *Artificial Organs* 40(11), 1071-1078.

Wang, C., P. Z. Gao, S. C. Tan and C. Xu (2012). Effect of aspect ratio on the laminar-to-turbulent transition in rectangular channel. *Annals of Nuclear Energy* 46(8), 90-96.

Wu, Y. L., S. H. Liu, H. J. Yuan and J. Shao (2011). PIV measurement on internal instantaneous flows of a centrifugal pump. *Science China-technological sciences* 54(2), 270-276.

Wu, Y. L., S. Li, S. H. Liu, H. S. Dou and Z. Qian (2013). *Vibration of Hydraulic Machinery*, Springer, Berlin.

Yan, B. H. (2011). Analysis of laminar to turbulent transition of pulsating flow in ocean environment with energy gradient method. *Annals of Nuclear Energy* 38(12), 2779-2786.

Zheng, L. L., H. S. Dou, W. Jiang, X. P. Chen, Z. C. Zhu and B. L. Cui (2016). Influence of rotor-stator interaction on flow stability in centrifugal pump based on energy gradient method. *International Journal of Turbo & Jet Engines*, 33(4), 413-419.

Zheng, L. L., H. S. Dou, X. P. Chen, Z. C. Zhu and B. L. Cui (2018). Pressure fluctuation generated by the interaction of blade and tongue. *Journal of Thermal Science* 27(1), 8-16.